Anisotropic polypropylene cellular polymers filled with nanoclays:

microstructure and properties.

A. Lopez-Gil [a,b], M. Benanti [b,c], E. Lopez-Gonzalez [b], J.L. Ruiz-Herrero [b], F. Briatico [c], M.A. Rodriguez-Perez [b]

[a]*CellMat Technologies S.L. CTTA. Paseo de Belén 9A, 47011, Valladolid, Spain.*

[b]*Cellular Materials Laboratory, (CellMat). Condensed Matter Physics Department, University of Valladolid, Paseo de Belén 7, 47011, Valladolid, Spain. Mail: marrod@fmc.uva.es*

[c]*Dipartimento di Chimica, Materiali e Ingegneria Chimica "Giulio Natta", Politecnico di Milano, piazza Leonardo da Vinci 32, 20133 Milano, Italy.*

Corresponding author: A. Lopez-Gil. Tel: +34 601326714. E-mail address: a.lopez@cellmattechnologies.com.

Abstract

This work deals with the production and characterization of low-density rigid foams (relative density < 0.2) with anisotropic cellular structures based on polypropylene filled with nanoclays, which present a high potential to be employed for structural applications. The anisotropy ratio, the cell size and the open cell content were modified by adding nanoclays and by applying different pressures during the foaming process. Moreover, nanoparticles catalysed the thermal decomposition reaction of the blowing agent, which involved the formation of bimodal cellular structures. The mechanical anisotropy of these foams was characterized by measuring the compressive modulus in three different directions. The experimental results were compared with those obtained theoretically by models that describe the mechanical response of anisotropic cellular structures.

Keywords

Foams, Nanoclays, Thermoplastic resin, Mechanical properties, Microstructures.

1- Introduction

Polypropylene (PP) is an ideal candidate to replace more common thermoplastics used for foaming applications such as polystyrene (PS) and polyethylene (PE) because of its high thermal stability, stiffness, strength and impact strength [1]. Several foamed products based on PP have been developed so far and they can be found in the market. The main example is expanded polypropylene (EPP), which is produced from a copolymer grade of PP by the *bead foaming process* and it is mainly used as shock energy absorber in automotive applications [2,3]. However, the stiffness and strength of the final foamed parts produced from EPP are low in comparison with those of other foamed materials employed for structural applications such as polyvinyl chloride (PVC), polyethylene terephthalate (PET) and polyurethane (PU) foams. The production of PP foams from linear isotactic grades would increase their stiffness and strength but this is a challenging task because of the low melt strength of this polymer. The development of branched grades allowed to broaden the foaming applications of this polymer [1] because when it is subjected to high expansions ratios, it experiences a sudden increase of viscosity caused by the entanglements of polymer chains (*strain-hardening phenomenon*). This phenomenon allows the production of PP foams with lower densities [4]. DOW produced the first foamed sheet based on a branched PP in 1994 [5] and since then, the production of PP foams from branched PP or blends with linear PP has spread worldwide. However, the foamed sheets conventionally produced by extrusion foaming present poor cellular structures (large cell sizes) [6-8], which still prevents their use in structural applications replacing PVC, PET and PU foams.

In order to improve the cellular structure and consequently, the mechanical properties of these branched PP-based foams several strategies can be adopted. One of them is the reinforcement of the polymer matrix with nanoclays because they not only increase the properties of the solid material but they are also able to promote significant alterations of the foaming mechanisms (nucleation, expansion and stabilization) [9]. These alterations could in turn result in positive modifications of the cellular structure from a structural point of view (cell size reduction, narrowing of the cell size distribution, etc.).

The literature dealing with PP foams reinforced with clays is abundant. Most of the works employed physical blowing agents such as CO_2 in an extrusion foaming process or in a batch-process carried out within an autoclave. The addition of clays in the extrusion foaming process even at very low contents (≤ 1 wt%) allowed increasing the expansion ratio of the foams [10-12]. The main reason given for this behaviour is the increment of the cell nucleation rates and the suppression of the cell coalescence mechanism by the addition of nanoclays. In the work of *Chaudhary, A.K. et al*, in which an extrusion process was also used but with a chemical blowing agent, the reason given for the better foaming behaviour of the nanocomposites is the induction of the strain-hardening phenomenon in a linear PP matrix [13]. The works in which the batch foaming process was employed gave rise to similar conclusions but the use of higher contents of clays produced some other interesting effects [14-19]. For instance, in the work of *Bhattacharya, S*. et al clay loadings in a branched PP above 4 wt% produced a decrease of the nucleation efficiency resulting in foams with larger cell sizes. In the work of *Nam, P.H. et al* the addition of 7.5 wt% of clays to a linear PP caused the formation of a bimodal distribution of cell sizes attributed to the presence of clay agglomerates. Other works employed different production routes. This is the case of the work of *Jiang, M et al*. in which the foams were produced by a two-stage injection foaming technique [20]. Moreover, *Antunes, M. et al* used a single-step compression moulding technique in which

azodicarbonamide was the blowing agent employed. This last work stated that clays produced an enhancement of the polymer thermal stability increasing the foaming window and reducing the time in which the polymer starts to expand [21]. The work of *Ma, Y. et al* was the only one in which the *improved compression moulding route* (*ICM*) was employed to produce PP foams reinforced with nanoclays [22]. However, it was mostly focused on the use of X-ray microtomography to analyse the cellular structure. The effect of nanoclays on the structure and in the mechanical properties obtained was not evaluated in detail.

In general, all the works mentioned lacked of an exhaustive study of the cellular structures obtained and they were highly influenced by the expansion ratio of the foams produced. Moreover, the relationship cellular structure-mechanical property was not analysed in detail. Last but not least, most of the foams obtained presented isotropic cellular structures because of the foaming method employed in which the expansion of the polymer is free.

A second strategy to improve the mechanical performance is to obtain foams with anisotropic cellular structures, whose mechanical properties are strongly dependent upon the direction in which they are measured. In general terms, the mechanical properties measured in the plane perpendicular to the direction where the cells are elongated are higher than in the equivalent isotropic structure (the same density). The *improved compression moulding route* (*ICM*) is a foaming process based on using *self-expandable moulds*, which allows the aforementioned anisotropic cellular structures to be obtained by simply modifying processing parameters and formulations [23-30].The degree of elongation of the cells can be quantified by the shape anisotropy (R), defined as the ratio between the maximum length of the cell and the minimum length in the perpendicular direction. In literature there are several models that attempt to describe the elastic response of polymeric foams under a compressive load [31-34], such as the model of cubic cell of *Gibson & Ashby*. *Huber & Gibson* modified the cubic cell

model with the aim of describing the behaviour of anisotropic foams [35]. They assumed a rectangular open cell instead of a cubic open cell and introduced the anisotropy ratio in the model equation.

From solid mechanics considerations previously reported [31,35], the ratio between the modulus in expansion direction E_{exp} and that of the transversal direction E_{trans} for an open cell foam is related to R by equation 1. In the case of closed cell foams equation 2 is valid, where f_s is the solid fraction contained in the cell edges and vertexes.

$$\frac{E_{exp}}{E_{transv}} = \frac{2R^2}{1+\left(\frac{1}{R^3}\right)} \tag{1}$$

$$\frac{E_{exp}}{E_{transv}} = f_s \frac{2R^2}{1+\left(\frac{1}{R^3}\right)} + (1-f_s)\frac{2R^2}{1+(1/R)} \tag{2}$$

The two models converge for values of f_s=1. The developed relations do not depend on the properties of the material (modulus of the solid polymer, E_s, and relative density, ρ_f/ρ_s) but only on the anisotropy of the equivalent rectangular cell (R).

These models estimate the mechanical behaviour of foams with very simple cell geometries such as cubes and rectangular prisms, which do not represent the real morphology of the cells. A more complicated cell geometry is the tetrakaidecahedron, which is known as the Kelvin cell model [36]. Several authors employed elongated tetrakaidecahedron with the aim of analysing non-isotropic foams [37,38]. *Sullivan et al* [39,40] defined a model for foams with f_s=1 (open cell foams) based on an elongated tetrakaidekahedron by specifying three independent dimensions and introducing an additional shape parameter called Q. The ratio of elastic modulus in the expansion direction (E_{exp}) to the modulus in the in-plane direction (E_{transv}) can be expressed as a function of R, Q and ρ_f/ρ_s by equation 3.

$$\frac{E_{exp}}{E_{transv}} = \frac{R^2}{4}\left[\frac{\left(2\widetilde{Q}^{\,2}R^2 + \frac{64Q^3}{\sqrt{16+\widetilde{Q}^{\,2}R^2}}\right)C_1 + \frac{8RC_2\widetilde{Q}^{\,3}\left(32+4Q\sqrt{16+\widetilde{Q}^{\,2}R^2}\right)}{\left(4Q+2\sqrt{16+\widetilde{Q}^{\,2}R^2}\right)(16+\widetilde{Q}^{\,2}R^2)}\left(\frac{\rho_f}{\rho_s}\right)}{16\,C_1 + \frac{8R^3C_2\widetilde{Q}^{\,5}}{\left(4Q+2\sqrt{16+\widetilde{Q}^{\,2}R^2}\right)(16+\widetilde{Q}^{\,2}R^2)}\left(\frac{\rho_f}{\rho_s}\right)}\right] \quad (3)$$

A more detailed explanation of the different parameters involved in the equation can be found in the works of *Sullivan et al*, in which the stiffness and strength ratios of several flexible and rigid foams with anisotropy ratios between 1 and 1.8 were compared with the anisotropic Kelvin model for three values of *Q* (1, $\sqrt{2}$ and 2) and for different relative densities. Moreover, in the work of *Hamilton et al* [41] low-density reinforced polyurethane foams with anisotropy ratios between 1 and 2 were evaluated by the *rectangular cell model* and the *modified Kelvin model*.

Taking into account the previous information the objectives of this work are firstly, the development of low relative density (ρ_f/ρ_s<0.2) pure and nanoreinforced PP foams with homogeneous cellular structures and good stiffness by the ICM route. Secondly, the study of the relationship between process (foaming pressure), structure (cell size, cell density, open cell content and anisotropy) and properties (compressive modulus) of the foams produced and how the presence of anisotropy and the incorporation of nanoclays affect this relationship. Finally, to evaluate if the models generally used for low density foams with elongated cells such as the *rectangular* and *Kelvin cell models* are adequate to predict the mechanical properties of anisotropic rigid foams of higher density such as the materials developed in this work.

2- Materials and methods

2.1- Materials

A branched high melt strength polypropylene (*PP Daploy WB135HMS*) provided by *Borealis* was employed as the polymer matrix. The nanoreinforcement employed was a

montmorillonite-type nanoclay organomodified with a quaternary ammonium salt (95 meq/100 g clay)provided by *Southern Clay Products*(*Cloisitie 20A*). A PP homopolymer modified with maleic anhydride (*Polybond 3200*) provided by *Chemtura* was used as the coupling agent. The chemical blowing agent employed was azodicarbonamide (ADC) *Porofor MC-1* provided by *Lanxess* with a decomposition temperature of 210ºC and an average particle size of 3.9 µm. A mixture of commercial antioxidants (*Irganox B561* and *Irgafos 168*), both supplied by *CIBA*, was added in all the formulations produced to prevent the thermal oxidation of the polymer.

2.2- Production

The production route is composed of two main processes: the compounding of the raw materials and the production of the foams by the improved compression moulding route (*ICM*). Firstly, two different formulations were produced: one without reinforcement (*PP*) and the other one based on polypropylene reinforced with nanoclays (*NP*), both blended with 2.5% of ADC. They were produced by melt-blending in a bench-top co-rotating twin-screw extruder *model ZK 25 T, Dr.Collin* that has five heating zones and a L/D of 24. The nanocomposite (*NP*) production was carried out prior to the incorporation of the blowing agent. Firstly, a masterbatch of nanoclays (50 wt%) and coupling agent (50 wt%) was produced. Both materials were manually mixed prior to being fed into the extruder. The temperature profile was set to 180-185-190-195-200 ºC and the screw speed to 50 rpm. The blend produced came out of the extruder die in the form of a molten strand which was immediately cooled by water, pelletized and finally dried in a vacuum oven at 60 ºC for at least 24 hours. The reason for drying the blend is the high susceptibility of both, nanoclays and the coupling agent to absorb water because of its hydrophilic chemical nature. Secondly, the *nanoclay-coupling agent* masterbatch was diluted with the branched polypropylene in order to produce the final nanocomposite (5 wt.% of nanoclays) in the same extruder and under the same production parameters.

Both, the non-reinforced material (*PP*) and the nanocomposite (*NP*), were melt blended with azodicarbonamide (2.5 wt%) and with a mixture of antioxidants (0.1 wt%) in the same extruder used for the production of the nanocomposite. The mixture of antioxidants is composed of *Irgafos168* (80 wt%) and *Irganox1010* (20 wt%). In this case, the temperature profile was set to 135-140-145-150-155 ºC and the screw speed to 120 rpm. The temperature is low enough in order to avoid a premature decomposition of the blowing agent. The molten compound obtained at the exit of the die was water cooled, pelletized and dried in a vacuum oven at 60 ºC for at least 24 hours. The compounds were extruded again under the same production parameters with the aim of obtaining a more homogeneous dispersion of ADC particles along the polymer. The materials obtained after the homogenization step were also dried under the same conditions previously described with the aim of avoiding the influence of water on the production of the foams.

Disc-shaped foams were produced by the *ICM* foaming route whose main feature is the use of a *self-expandable mould* (150 mm diameter). The mould and the main steps involved in this foaming route are shown in Figure 1. The axis on the right was included to specify the expansion direction (D_1) and the direction perpendicular to it (D_2). The moulds are *self-expandable* because the piston (1) moves up pushed by the expanding polymer immediately after releasing the pressure. The total distance covered by the polymer during its expansion is established by a built-in blocking system (2) in which a metallic ring (3) of a determined height is used to set the foam expansion ratio. The final foam density can be adjusted by simply replacing the metallic ring for another of a different height. Moreover, the molten polymer is retained inside the mould cavity not only during the application of the pressure but also during the expansion process because the mould is hermetically sealed by rubber joints (4) allowing the production of non-crosslinked foams with defined shapes, discs in this particular case.

The process is split up into several steps. First of all, a certain amount of foamable compounded pellets (5), enough to fill the mould cavity and to reach the final foam density are placed into the mould cavity (Figure 1a). Then the mould is closed and placed between the hot plates of an hydraulic press, which is used to apply heat and pressure simultaneously. Secondly, pressure and temperature are applied for 15 minutes for all the foams produced (Figure 1b). After this time, during which the entire blowing agent decomposes (b), the applied pressure is reduced, producing the nucleation and growth of the cells (Figure 1c). Thirdly, the expansion of the polymer is limited by the built-in blocking system (2), which allows foamed discs of 10 mm in thickness and 150 mm in diameter to be obtained with the target foam density (6). The mould is finally immersed in water in order to cool and stabilize the foam.

The temperature and pressure conditions employed to produce the foams are summarized in Table 1. The denomination of the materials in the first column indicates the formulation (*PP* or *NP*) and the pressure conditions. Different pressures from 0.5 to 8 MPa were used for both formulations. Moreover, the foaming temperatures used were different because the addition of nanoclays accelerated the blowing agent decomposition process involving the generation of a higher amount of gas (this will be explained later in the section 5.1). Therefore, the temperature used for the NP formulation was 10 C lower than that used with the PP formulation.

Foam sample	Temperature (C)	Pressure (MPa)
PP0.5	200	0.5
PP1.5	200	1.5
PP4	200	4
PP8	200	8
NP0.5	190	0.5
NP1.5	190	1.5
NP4	190	4
NP8	190	8

Table 1. Foams produced and production parameters.

2.3- Characterization

2.3.1- Thermogravimetric analyses

A thermogravimetric analyser model TGA/SDTA 861 was used to perform two kinds of experiments over the solid formulations (PP and NP): a *dynamic analysis* and *isotherms*. On the one hand, in the *dynamic analysis* the samples were heated from 50°C to 1000 °C at 20 °C/min under N_2 atmosphere (60 cm^3/min). On the other hand, in the *isothermal program* the samples were heated from 50 to 190 °C (NP) and from 50 to 200 °C (PP) at 20 °C/min under N_2 atmosphere (60 cm^3/min). The final temperatures (190 and 200 °C), which correspond to the foaming temperatures (Table 1), were maintained constant for about 30 minutes in an effort to simulate the foaming process. Three samples of each formulation were measured in order to evaluate the reproducibility of the results obtained.

2.3.2- Density

Density (ρ_f) was determined on each foamed specimen following the ASTM standard D1622-14. The density of the solid polymer (ρ_s) was measured using a gas pycnometer. The measured density of the pure formulation pellets (PP) was 0.90±0.01 g/cm^3 while that of the nanoreinforced formulation (NP) was slightly higher 0.92±0.02 g/cm^3.

2.3.3- Open cell content

A gas pycnometer model *AccuPyc II 1340 Micromeritics* was used for the open cell content (OC) measurements following the standard *ASTM D6226-10*. Cubic samples (20x20x10 mm^3) extracted from each kind of foam were used for the experiments. Five measurements were carried out on each kind of foam. Equation 4 was employed to calculate the open cell content.

$$OC = \frac{V - (2V_1 - V_2)}{V(V_f)} x100 \quad (4)$$

Where *V* represents the geometric volume of the sample, V_1 is the volume of the cubic sample measured by the gas pycnometer and V_2 is the volume of the same cubic sample after being cut in two planes according to the standard. By using this method, it was possible to obtain a more accurate value of the open cell content without considering the cells located on the surface, which were open because the sample had to be cut in order to be extracted from the foamed disc. Finally, V_f is the porosity of the foamed sample, which was calculated by equation 5.

$$V_f = 1 - \frac{\rho_f}{\rho_s} \quad (5)$$

Where ρ_s and ρ_f are the density of the solid and the foam, respectively.

2.3.4- Microstructure characterization

SEM micrographs of the foams were taken in a plane parallel to expansion direction (D_1/D_2) and in the plane perpendicular to it using a scanning electron microscope model *Jeol JSM-820* (2–20kV and 10^{-9}-10^{-10}A). The samples (10x10x10 mm^3cubes) were previously prepared by cutting with a razor-sharp blade along the two planes previously specified and they were made conductive by a sputtering deposition of gold. Images were digitalized with a resolution of 1200 dpi. 3-5 images along the expansion plane (D_1/D_2) were taken at high magnification and later joined with *Photoshop CS7* in order to obtain high-resolution images of the entire thickness (≈10mm) of the foamed samples. Some examples of these images are shown in Figure 6.

The cellular structure was characterized in two dimensions (in the images obtained from the expansion plane) by means of an image analysis tool based on the software Image J that allows the user to control the selection of cells to be measured [42]. Before the image analysis process the contour of each cell was marked in order to enhance the contrast and increase the

accuracy of the analysis (Figure 2a).The cell size of each cell was defined as the average of the diameters measured in four different directions (0°, 90°, ±45°). The average foam cell size (Φ) is therefore, calculated as the average cell size of all the cells considered in the analysis as shown in equation 6 in which *n* represents the total number of cells.

$$\Phi = \frac{\sum_{i=1}^{n} \Phi_i}{n} \tag{6}$$

The cell size in the expansion direction (Φ_{i1}) and in the transversal direction (Φ_{i2}) for each cell was also measured as shown in Figure 2b in which the cell is theoretically represented as an ellipse. The average values for all the cells considered in the analysis was also calculated and expressed as Φ_1 and Φ_2 for the expansion and transversal directions, respectively. In addition, an image pixels count allows computing the area occupied by each cell (as indicated in Figure 2c as A_{cell}).

The Asymmetry Coefficient (*AC*) of the cell size distribution was calculated by employing equation 7 in which *SD* is the standard deviation of the cell size distribution calculated by equation 8.

$$AC = \frac{\sum_{i}^{n} (\Phi_i - \Phi)^3}{n(SD)^3} \tag{7}$$

$$SD = \frac{\sqrt{\sum_{i}^{n} (\Phi_i - \Phi)^2}}{n - 1} \tag{8}$$

The homogeneity of the cell size distributions is described by the parameter *NSD* (normalized standard deviation), which is the ratio between *SD* and the average cell size, as expressed by equation 9.

$$NSD = \frac{SD}{\Phi} \tag{9}$$

The cell density (N_v) is defined by equation 10 where A is the image area, n is the total number of cells contained in that area and M is the magnification factor of the micrograph [43,44].

$$N_v = \left[\frac{(nM^2)}{A}\right]^{3/2} \tag{10}$$

Anisotropy ratio R_i for each cell is calculated by equation 11.

$$R_i = \frac{\Phi_{i1}}{\Phi_{i2}} \tag{11}$$

Anisotropy ratio of the whole specimen is calculated in two ways. On the one hand, as the arithmetical average of R_i for all the cells considered in the analyses and on the other hand, as the weighted average (R_w) over the cells area, as shown in equations 12 and 13, respectively.

$$R = \frac{1}{n}\sum_i R_i \tag{12}$$

$$R_w = \frac{1}{A_{cell}}\sum_i R_i A_i \tag{13}$$

Where n is the total number of cells, A_i is the area occupied by each cell and A_{cell} is the total area occupied by the cells in the analysed image. ($A_{cell} = \sum_i A_i$)

2.3.5- Mechanical characterization

Compression tests were performed using a *mod. 5500R-6025 Instron universal machine* equipped with a 100 N load cell and compression plates. The displacement was measured by means of an extensometer. A constant strain rate of 1.6×10^{-3} s^{-1} was used. Three cubic samples (10x10x10 mm^3) were extracted from each kind of foam and tested at small strains (0-3%). As the overall strain proved to be completely recovered after each test, each sample was tested

in the expansion direction (D_1) and in two transverse directions (D_2, D_3) as schematically represented in Figure 3.

All tests were conducted after materials had been conditioned at 23±1°C for at least 24h. Elastic modulus (E) was calculated as the slope of the linear part of the stress-strain curve. Friction between plates and sample surfaces was regarded as non-influent. Modulus in each direction was calculated as the average of all the measurements.

3-Results and discussion

3.1- Thermal characterization of solid formulations

The solid formulations produced (PP and NP) were thermally characterized by TGA in order to evaluate how the presence of nanoclays affects both, the thermal decomposition of the blowing agent and the thermal stability of the polymer matrix. This was accomplished by a dynamic scan (temperature scan) and by isotherm scans performed at the same temperature of the foaming process. The dynamic analysis is shown in Figure 4.

Figure 4 includes two plots. The one on the left (a) shows the *dynamic scan* in all the range of temperatures studied (50-1000ºC) in which two main weight losses are observed. The first one is linked to the blowing agent decomposition. The second one is connected to the thermal degradation of the polymer matrix. Both weight losses were marked with circles on the plot. The one on the right is the same plot but focused on a narrower range of temperatures (150-400ºC) with the aim of observing in more detail the weight loss associated to the blowing agent decomposition reaction. The onset of the decomposition reaction was measured (see tangent lines to curves on Figure 4b). This onset denotes the moment in which the decomposition reaction in gases starts to take place. The ADC onsets obtained for both formulations (NP and PP) are observed in Table 2, together with the onset corresponding to the thermal degradation of the polymer (obtained in the same way), the total weight loss

associated to the blowing agent decomposition reaction and the percentage of residues left after the test.

Formulation	ADC onset (ºC)	ADC weight loss (%)	Polymer onset (ºC)	Residue (%)
PP	217,5 ± 1,7	2,57 ± 0,01	397,7 ± 1,3	1,02 ± 0,31
NP	197,7 ± 1,3	2,60 ± 0,17	425,7 ± 4,0	3,80 ± 0,64

Table 2. Parameters obtained from the dynamic TGAs.

The ADC onset is clearly lower for the formulation NP (PP reinforced with nanoclays), which indicates that nanoclays are catalysing the decomposition reaction of the blowing agent. This is why the foaming temperature was lowered 10 ºC in the case of the NP formulation (Table 1). The total weight loss associated to the blowing agent decomposition reaction is very similar for both formulations, which is logical taking into account that they were produced by adding the same amount of blowing agent (2,5wt%). However, the curves are different. In the case of the PP formulation, the drop is not gradual and takes place in three stages. The first stage (1) (Figure 2b) corresponds to the exothermic thermal decomposition in gases and the following two (2 and 3) correspond to the endothermic decomposition of the solid products which were generated after the first reaction [45]. Another interesting effect was found in the thermal degradation of the polymer. The onset of the NP formulation (425,7ºC) is higher than that of PP (397,7 ºC). Therefore, nanoclays are not only catalysing the ADC decomposition reaction but are also providing the polymer with higher stability in the molten state at high temperatures. Finally, the total amount of residues found in the NP formulation (3,8 %) is higher than that found in the PP formulation (1,02 %). The difference is attributed to the presence of clays. However, the amount of residues is lower than the initial amount of nanoparticles added in the formulation (5 wt%) which is partly due to the loss of the organomodification (quaternary ammonium salts) during the thermal process.

Figure 5 includes the isotherms performed at 190 and 200 ˚C over the NP and PP formulations, respectively. This analysis was carried out in order to evaluate in more detail the catalytic effect of nanoparticles.

The plot on the left (a) shows the complete isotherms while the plot on the right (b) shows a zoom over the period of time in which both formulations start to lose weight. This moment was denominated as a *time onset* and it was obtained in the same way as the ADC onset (Figure 5b). The *time onsets* for both formulations are observed in Table 3 along with the weight loss at 900 s, which corresponds to the foaming time, and with the weight loss at the end of the analysis (2250 s).

Formulation	Time onset (s)	Weight loss at 900 s (%)	Total weight loss (%)
PP	477 ± 11	$0{,}76 \pm 0{,}02$	$1{,}44 \pm 0{,}03$
NP	354 ± 6	$1{,}33 \pm 0{,}05$	$1{,}68 \pm 0{,}01$

Table 3. Parameters obtained from the isotherms.

The time onset of the NP formulation (348 s) is lower than that of the PP formulation (477s) even though the isotherm of the NP formulation was performed at a lower temperature (190 ˚C). This fact confirms the strong catalytic effect of the nanoclays over the blowing agent decomposition reaction. Not only ADC starts to react earlier but also the decomposition reaction is faster. This is observed in the slope of the NP curve, which is more pronounced than that of the PP curve. The previous facts involved a clearly higher amount of ADC decomposed at 900 s (foaming time) in the NP formulation (weight loss at 900s). This is also reflected at the end of the isotherm where the amount of ADC decomposed in the NP formulation (1,68 %) is still higher than that decomposed in the PP formulation (1,44%). In spite of the fact that the total amount of ADC blended with the polymer matrix was 2,5wt%, the total weight loss registered at the end of the isotherms was lower. This is because at the temperatures at which the isotherms were performed not all the reactions involved in the ADC decomposition are

completed, especially those linked to the decomposition of the solid products which are generated after the first reaction (see Figure 4b).

3.2- Microstructure

Some examples of the typical cellular structure of the studied foams in a plane parallel to the expansion direction (D_1/D_2) and in the plane perpendicular to it is shown in Figure 6. All the pure PP foams present cellular structures, which are very similar to the one shown in Figure 6a. It is characterized by elongated cells in the expansion direction (D_1). Conversely, NP foams present cellular structures that differ with moulding pressure. On the one hand, the material prepared with the lowest pressure, *NP0.5*, (Figure 6b) presents a large number of small and almost spherical cells together with a small number of large cells, which are elongated in the expansion direction. The small cells are randomly distributed in the walls of the larger ones. On the other hand, the foam *NP8* (Figure 6c) which was prepared with the highest pressure, presents a more homogenous cell size distribution. The images taken in a plane perpendicular to the expansion direction (Figure 6d-f) show that cells are essentially axial-symmetric in D_1 direction. This means that no significant differences are expected between the properties measured in directions D_2 and D_3. The reason why some of the foams produced present elongated cells is that the expansion was restricted in D_1, which coincides with the expansion direction as shown in Figure 1.

It is interesting to note that some cells, specifically those located in the upper and lower parts of the foamed disks, are elongated in another direction which is different from D_1. The reason could be that the cells in the inner part continued growing even after the foam filled the mould (and up to the complete stabilization of the cellular structure) due to the occurrence of temperature gradients during cooling. As the cells located near the upper and lower mould cavity surfaces did not have space to grow, they were deformed by the inner cells

in such way that they were finally elongated in another direction different from D_1. The cell size distributions (bin size: 25 μm) for the 8 studied foams (*PP* and *NP*) is reported in Figures 7 and 8.

The cumulative curves of both, the area occupied by the cells and the number of cells are represented in Figure 9. In addition, all the average parameters obtained after a detailed image analyses of the cellular structures are shown in Table 4.

Materials	Density (kg/m^3)	Φ (μm)	AC_Φ	NSD_Φ	N_v(cells/cm^3)	*OC* (%)
PP0.5	173	193.2	0.63	0.62	$10.3 \cdot 10^4$	32.3
PP1.5	183	205.1	0.33	0.61	$8.15 \cdot 10^4$	35.0
PP4	182	219.5	0.42	0.57	$7.1 \cdot 10^4$	26.3
PP8	188	230.7	0.34	0.41	$6.1 \cdot 10^4$	13.5
NP0.5	182	125.1	2.52	1.37	$38.1 \cdot 10^4$	53.6
NP1.5	181	173.8	1.38	0.94	$14.1 \cdot 10^4$	84.2
NP4	189	156.0	0.90	0.52	$19.6 \cdot 10^4$	91.9
NP8	180	118.2	1.26	0.47	$45.09 \cdot 10^4$	91.8

Table 4. Average parameters of the cellular structure and open cell content.

The density of all the foams produced is very similar (Table 4), regardless of the formulation employed and the pressure applied. This fact allows evaluating the cellular structure without the influence of the expansion ratio. All the *PP* foams appear to be very similar regarding the cell size distributions (Figure 7). This is confirmed in the cumulative distributions, both for cell number and cell area, which nearly superimpose each other (solid lines of Figure 9). On the contrary, the *NP* ones present very different trends in terms of the pressure applied, not only in the cell size distributions (Figure 8) but also in the cumulative curves (dashed lines of Figure 9) confirming what was shown qualitatively by SEM images in Figure 6.

One interesting feature of the foams developed, especially in the nanoreinforced foams, is the presence of mesoporosity (small cells within the cell walls of the larger ones), which can be quantitatively estimated from the previous plots. For instance, in the foam produced with

the lowest pressure (*NP0.5*) about 80% of the cells have sizes below 100µm. However, the area that these cells occupy is below 10% constituting the reason why they can be considered as mesoporosity (i.e. the porosity of the solid frame). This mesoporosity tends to disappear when increasing the foaming pressure and the distribution tends to get narrower (Figure 8c and d).For instance, on the left side of the distribution the number of cells with sizes below 50 µm goes from more than 40% in *NP0.5* to less than 5% in *NP8*, while on the right side, cells with sizes larger than 300 µm represent more than 12% in *NP0.5* while only 1% in *NP8*.

The shape of the cell size distributions is measured by the *AC* values (asymmetry coefficient), which are shown in Table 4. The *AC* of the *NP0.5* foam, for instance, is very high (2.52) indicating a non-symmetric distribution with few large cells whose size are far from the average value. On the contrary, as pressure increases the *AC* values decrease and hence, the distributions tend to be more symmetric. In general, the cell size distribution symmetry of the *PP* foams is higher than those of the *NP* foams because their *AC* values are lower. NSD is also sensitive to the presence of the clay particles. In fact, the presence of this phase increases this parameter, especially for the foams with a bimodal cell size distribution.

Therefore, the cellular structures of these foams were influenced by two factors: on the one hand, by the addition of nanoclays and on the other hand, by the pressure applied during foaming. Both aspects are discussed in more detail the following sections.

3.2.1- Influence of nanoclays

The addition of nanoclays clearly influenced the cell size (Φ) and cell density values (N_v).The average cell size of all the NP foams is 143,3 µm while that of the pure foams is 212,1µm. The same result is observed for the N_v values but in an opposite way, as the average value of *NP* foams ($2.9 \cdot 10^5$) is higher than that of *PP* foams ($7.9 \cdot 10^4$). This is possibly due to a heterogeneous nucleation of cells caused by the presence of nanoclays in the molten polymer.

The energy barrier that gas molecules have to overcome to form a single cell on the surface of a nanoclay particle is lower than that required in the molten polymer [9]. Nanoclays also influenced the level of interconnectivity between cells. In general the *OC* values of the *NP* foams are higher than that of the *PP* foams. This is confirmed by observing the cellular structure morphology of a reinforced foam (*NP1.5*) in Figure 10.

The cellular structure of the *NP1.5* foam shows a high number of interconnections between cells in the form of holes and ruptures within the cell walls which are indicated in the image by black arrows, confirming what was measured by gas picnometry (*OC=84.2%*). On the contrary, the number of interconnections in the pure foam is considerably lower (*OC=35%)*. In spite of the high interconnectivity levels of the *NP* foams, the cells are still supported by walls. Nevertheless, these walls present small holes, which are responsible for the high open cell content values. The formation of this structure could be caused by a higher cell wall thinning during expansion. At some specific expansion ratio during the foaming process the cell wall membrane is so thin that it breaks, thus producing the holes and ruptures observed in Figure 9. It seems that the presence of clays could affect the rheological behaviour of the molten polymer. Branched PPs present the strain-hardening phenomenon by which the molten polymer experiences a sudden increase of extensional viscosity when stretched at high strains (as in a foaming process) [46]. However the presence of clays reduces this effect. This was observed in previous works in literature [47]. This fact would make the cell walls in NP foams less capable of supporting the pressure of the gas during expansion and as a consequence they break interconnecting the correspondent cells sharing the wall.

3.2.2- Influence of foaming pressure

The pressure applied over the *polymer/blowing agent* system also affected the cellular structures obtained. This processing parameter is very important in foaming processes because it determines the amount of blowing agent dissolved in the molten polymer prior to the expansion stage [48]. Nevertheless, PP foams do not seem to be influenced by pressure because both, Φ and N_v, are very similar (this was also observed in the cell size distributions of Figure 6). There is a slight tendency for the cell size to increase and the cell density to decrease on increasing pressure, but these variations are negligible when compared with those produced in *NP* foams. In this case, the cell density values drastically fall when the pressure is shifted from 0.5 MPa to 1.5 MPa. In fact, the general trend obtained with *NP* foams is rather contradictory because the highest cell density values were obtained with the foams produced at the lowest (0.5 MPa) and the highest (8 MPa) pressures. However, the cellular structure morphology of these foams is very different. *NP0.5* is characterized for presenting a bimodal distribution of cell sizes while *NP8* is characterized for presenting a more homogeneous structure with a narrower cell size distribution. This is confirmed by the *NSD* values, which progressively decrease as the pressure increases.

An explanation for this behaviour was found in the TGA measurements previously performed over the two solid formulations (PP and NP). Figure 4 showed a clear reduction of the temperature (ADC onset) at which the blowing agent starts to decompose when adding nanoclays. The foaming temperature was decreased when using the NP formulation (190ºC) in order to compensate for this effect and to generate the same amount of gas in the two formulations. Nevertheless, the results obtained with the isotherms (Figure 5) indicated that the blowing agent in the presence of nanoclays, even after decreasing the foaming temperature 10ºC, was able to generate a higher amount of gas than in the pure formulation (weight loss at 900 s) (Table 3).

This fact is consistent with the cellular structures obtained. In the case of the pure formulations, all the gas generated was able to be dissolved within the molten polymer in all the range of external pressures studied (from 0.5 to 8 MPa). For this reason, the cellular structures obtained are very similar. However, the amount of gas generated in the nanoreinforced formulations (NP) was higher, which made the *polymer/blowing agent* system more sensitive to pressure variations. This means that the amount of gas dissolved at high pressures (8 MPa) could be higher than that dissolved at low pressures (0.5 MPa). The cell size and cell density are parameters of the cellular structure, which depend on the amount of gas dissolved within the polymer. The higher the amount of gas dissolved the higher the nucleation rate and as a consequence, the number of cells in the final foam. This is why the cell density and cell size values obtained with the NP varied according to the pressure exerted.

An additional effect, in combination with the previous one, could explain the formation of the bimodal cell size distributions in the NP foams. The gas molecules, which could not be dissolved into the polymer matrix when employing low external pressures, formed cells even before releasing the external pressure applied. This involved a foaming process with two nucleating stages. A few cells nucleated in a first step (during the application of the external pressure) and hence, they had more time to grow, resulting in the formation of large cells, while most of the cells nucleated in a second stage (after releasing the external pressure) with less space and time to grow and therefore, creating smaller sizes. A similar effect was observed in a previous work in which a two-step depressurization batch process was used for the formation of a bimodal cellular structure but in this case using polystyrene foams and CO_2 as the physical blowing agent [49].

The open cell content is another parameter, which is also connected with the amount of gas dissolved. In the NP foams produced at high pressures, the amount of gas dissolved into the molten polymer grows and therefore, the pressure inside the cells in the expansion

process is higher, making the cell walls more prone to break. The results in Table 4 confirm the previous hypothesis because the foams NP4 and NP8 present higher OC values.

3.2.3- Anisotropy evaluation

Table 5 reports the average values of cell size in the expansion direction (Φ_1) and in the transversal direction(Φ_2) for all the studied foams. The average anisotropy ratio *R* (calculated using equation 12) and the average anisotropy ratio weighted over the area of each cell R_w (calculated using equation 13), are also shown.

Materials	Φ_1 (μm)	Φ_2(μm)	*R*	R_w
PP0.5	159.0±126	111.2±81	1.43±0.66	1.49±1.61
PP1.5	165.4±113	111.8±75	1.48±1	1.54±0.87
PP4	179.9±108	124.9±73	1.41±0.58	1.49±0.41
PP8	202.4±88	158.1±67	1.28±0.61	1.35 ±0.63
NP0.5	106.5±131	78.9±123	1.35±0.55	1.75±0.49
NP1.5	144.2±151	102.3±104	1.41±0.57	1.64±0.32
NP4	145.1±94	126.2±72	1.15±0.42	1.09±0.56
NP8	101.5±82	76.3±76	1.33±0.45	1.26 ±0.43

Table 5.Average cell size in the expansion (Φ_1) and transversal (Φ_2) directions. Average anisotropy ratio in the expansion direction *R*(equation 12)and R_w (equation 13).

The results show that in all the cases, $\Phi_1 > \Phi_2$ and hence, $R > 1$. This indicates that all the foams produced present anisotropic structures, which is consistent with the fact that the expansion of the polymer was restricted to only one direction (D_1). However, the degree of anisotropy and the tendencies with respect to the pressure applied seem to change when the anisotropy ratio of each cell is weighted with their correspondent occupied area. The plots of Figure 11 show the values of *R* and R_w for all the *PP* and *NP* foams.

There is no apparent trend regarding foaming pressure when only the *R* values are considered and in general the *NP* foams present lower anisotropy ratios that the *PP* foams. This is caused by the great number of small cells present in the NP foams produced with the lower pressures, which are isotropic. On the contrary, when considering R_w a clear trend appears in the case of the *NP* foams. The R_w values of the foams produced with the lower

pressures (*NP0.5* and *NP1.5*) are clearly higher than those of the correspondent pure foams (*PP0.5* and *PP1.5*) and they seem to decrease with the applied pressure. The results of R_w seem to be consistent with the cellular structures shown in Figure 6 and with the explanation given before for the formation of the bimodal cell size distributions. The foaming process of the NP foams produced at low pressures is controlled by two nucleation stages. The cells formed during the first nucleation stage not only had more time to grow but also more space and therefore, they could grow with a greater elongation. However, the cells formed during the second stage, had less space and less time. As a consequence they became practically isotropic.

Although no unique correlation is observable, it can be supposed that different combinations of *R* and cell size will have a different influence on the mechanical behaviour of foams. In fact, according to the classic beam theory, that has been used to analyse the deformation mechanisms in cellular materials, the elastic deformation of cells depends on the third power of their size. This means that bigger cells contribute much more than smaller ones to specimen deformation [50] and their anisotropy has a greater influence on the elastic modulus of the material. For this reason R_w is then considered to better represent the anisotropic structure of the materials. The results of the next section will prove that this assumption is correct.

3.3- Mechanical behaviour

Foamed structures subjected to small deformations react elastically with a modulus dependant on its microstructure and, in the case of anisotropic foams, on the direction of the load. The results of the mechanical tests are summarized in Table 6. The E_{exp} values represent the average over the moduli measurements in the expansion direction (D_1). E_2 and E_3 are the averages of the moduli in the transversal directions measured on the samples along directions

D_2 and D_3. In most of the analysed materials, $E_2 \approx E_3$, hence, their average (E_{transv}) is taken as the modulus of the materials in the transversal direction. The ratio of modulus (E_{exp}/E_{transv}) is reported too and indicates the mechanical anisotropy of the material.

Material	E_{exp}[MPa]	E_2 [MPa]	E_3[MPa]	E_{transv}[MPa]	E_{exp}/E_{transv}
PP0.5	81.4±1.2	32.7±4.1	33.8±1.4	33.2±4.3	2.4±0.3
PP1.5	96.2±1.3	33.8±3.2	39.4±4.1	36.6±5.2	2.6±0.4
PP4	96±5.7	39±2.8	44±1.6	41.5±3.2	2.3±0.2
PP8	66.3±2.6	30.6±0.8	44±1.3	37.3±1.6	1.8±0.1
NP0.5	134.4±7.7	33±4.4	55±2.7	44.0±5.2	3.0±0.4
NP1.5	118.3±4.9	50.1±6.5	44.4±2.5	47.2±6.9	2.5±0.4
NP4	73.2±8.4	47.6±2.5	48.5±4.5	48.0±5.2	1.5±0.2
NP8	78±5.4	33.4±3.2	30±3.8	31.7±10.4	2.5±0.8

Table 6. Compressive moduli values.

Figure 12 represents both, the E_{exp} and the E_{transv} values, as a function of R_w for all the foams produced.

These plots prove that R_w has a clear influence on the elastic modulus when the foams are measured in the expansion direction (E_{exp}). The trend obtained indicates that the elastic modulus increases with the R_w values. Therefore, the large anisotropic cells characteristic of the NP foams produced at low pressures have a significant influence on the measured mechanical properties. In the case of the measurements performed in the transversal direction (E_{transv}) there is not any apparent trend with R_w. However, in this direction (E_{transv}) it is possible to observe that practically all the NP foams present higher values of the modulus than the PP foams. This fact proves the reinforcing effect of nanoclays on the polymer matrix within the cell walls and struts because even though they promote high levels of interconnectivity in these foams (Table 4), the modulus obtained are higher.

Mechanical properties can be correlated with structural characteristics of the materials by means of the models presented in the introductory section. Those models demonstrated to be predictive of the behaviour of cellular materials as long as they follow these conditions: periodicity of the cellular structure, narrow cell size distributions, low relative density and

open cell structures [35,39]. The materials which are the object of this investigation only partly satisfy these conditions. It is nonetheless also worth attempting to apply the models also to polymer foams with higher densities and partially open cell structures, like the PP-based ones produced in this work. In Figure 13a the experimental data for stiffness ratio (E_{exp}/E_{transv}) are compared with the *Huber & Gibson* relation for open cell foams (f_s=1) obtained using equation 1 and with the *Huber &Gibson* relation for closed cell foams (equation 2) and different values of f_s. In Figure 13b the comparison is carried out with the prediction given by the *elongated Kelvin cell model* with different values of *Q* obtained using equation 3 (dashed lines) [39]. The elongated *Kelvin* cell model curves are calculated for different values of *Q* (2, $\sqrt{2}$, 1) and for a relative density similar to that of the studied foams (ρ_f/ρ_s= 0.19).

These analytical models fit well with the experimental results for NP foams when considering low R_w values but they failed to describe the mechanical behaviour of foams with $R_w > 1.6$. On the one hand, the NP foams produced at high pressures (R_w=1,09 and 1,26) fit well with the Huber-Gibson model for open cell foams. These foams satisfy two conditions of the model because they present highly homogeneous cell size distributions and high open cell contents. On the other hand, the PP foams seem to follow the trend marked by the Huber-Gibson model for closed cell foams when f_s is in between 0.3 and 0.4. This is in good agreement with the fact that the pure foams present low open cell contents. However, they also fit well with the Kelvin model when $Q = \sqrt{2}$, which describes the mechanical behaviour of open cell foams. This may be caused by the possibility of adjusting the model with the morphological parameter Q. On the contrary, when considering high R_w values (R_w>1.6) the models do not follow the trend marked by the experimental values. This could be due to the presence of bimodal cell size distributions, which make the cellular structure of these foams non periodic and non-homogeneous. Therefore, it seems to be necessary to adjust the previous models or to develop new ones in order to be able to describe properly the

mechanical properties of these medium-low density foams with non-homogeneous cell size distributions.

4- Conclusions

The use of the ICM technology allowed the production of PP foams with densities lower than 0.2 g/cm^3 and with very different cellular structures depending on the pressure applied and on the presence of nanoclays in the formulations. Cellular structure parameters such as cell size, cell density, anisotropy ratio, etc. were accurately measured by means of an user-interactive digital image software that allowed a proper correlation of these parameters with the mechanical properties obtained.

The presence of nanoclays not only promoted heterogeneous nucleation of cells (cell size was reduced) but also induced a catalytic effect in the blowing agent decomposition reaction, which involved the generation of higher amounts of gas and the formation of a bimodal cell size distribution (mesoporosity) in the specimens produced at the lowest pressures. A two-stage nucleation process could be the reason underlying the presence of two populations of cells, in which the large cells nucleated in the first stage and the small cells, but more numerous, in the second stage. Moreover, nanoclays induced ruptures of the cell walls producing partially open cellular structures.

The unidirectional expansion of the polymer in the ICM process promoted the formation of anisotropic cellular structures. Cells anisotropy was analysed and different trends for each material were observed. In particular, it was noted that the smaller cells of the NP foams (mesporosity) tend to have rounded shape. Taking into consideration this fact, anisotropy ratio weighted over the cell area (R_w) was taken as being a more representative parameter of the foam structure.

These morphological changes had a measurable effect on the elastic moduli of the foams measured in compression, which reflected the structural anisotropy morphologically observed. The modulus in the expansion direction is, in fact, higher than that in the transversal

direction in all the studied foams and there is a clear relation between the modulus measured in the expansion direction and the cellular anisotropy. Moreover, the incorporation of clays, apart from the previously mentioned modification of the cellular structure allowed the improvement of the elastic mechanical properties in all the analysed directions.

Lastly, the application of two different micromechanical relations, based on two different cells (rectangular and tetrakaidecahedron cell), was attempted. Acceptable correspondence between experimental data and the *Huber-Gibson* model, both for open cell and closed cell foams, was obtained when considering low R_w because in this case, the cellular structures are more homogeneous in terms of cell size distribution satisfying one of the main conditions of this model. However, in the case of the foams with the bimodal cell size distribution there was not a good correlation, which could be due to the non-periodicity and lack of homogeneity in these structures.

Acknowledgements

Financial assistance from MCINN (MAT2009-14001-C02-01 and MAT 2012-34901), the Junta of Castile and Leon (VA035U13) and the FPI grant Ref: BES-2010-038746 (A. Lopez-Gil) is gratefully acknowledged.

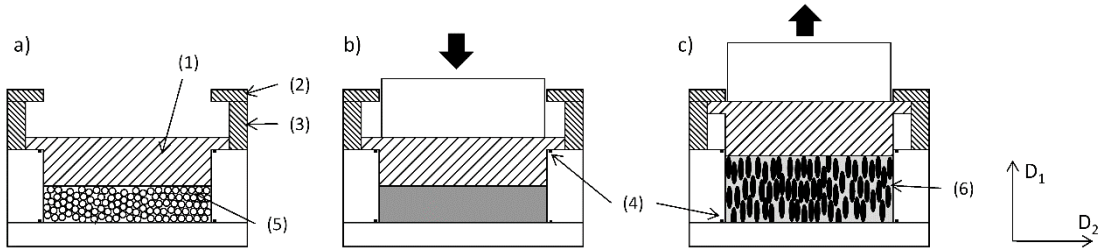

Figure 1: ICM foaming process. (a) The mould with the pellets inside prior to the foaming process. (b) The mould with the molten material inside during the time in which pressure and temperature are applied. (c) The mould with the foam inside after releasing the pressure.

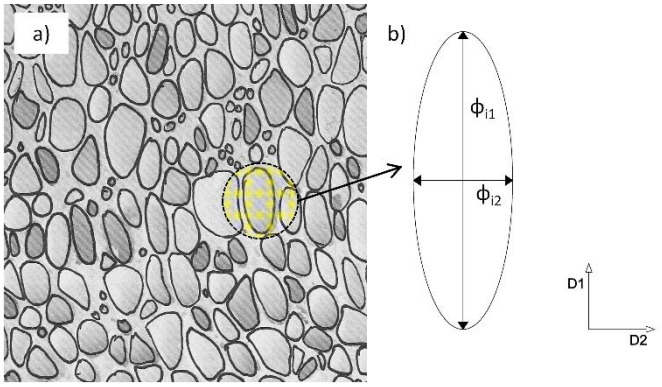

Figure 2: (a) Part of an image before digital analysis with outlined border of cells. (b) Cell size in the expansion (D1) and transversal directions (D2).

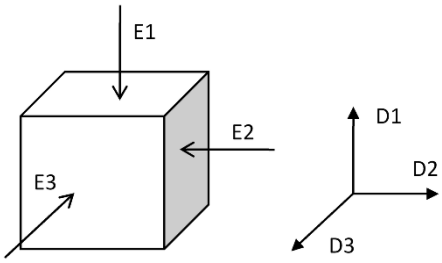

Figure 3: Scheme of the cubic PP foamed samples and the directions in which the compressive modulus (E) was measured.

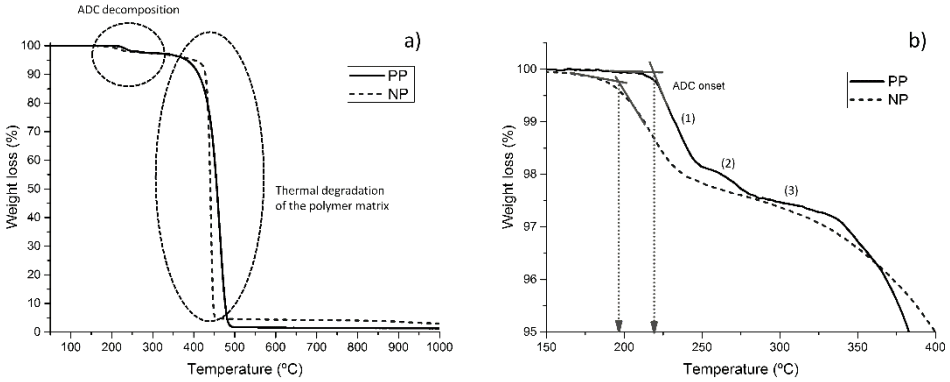

Figure 4: TGA dynamic analyses. (a) All the range of temperatures (50–1,0008C). (b) A range of temperatures (150–4008C) focused on the ADC decomposition temperature.

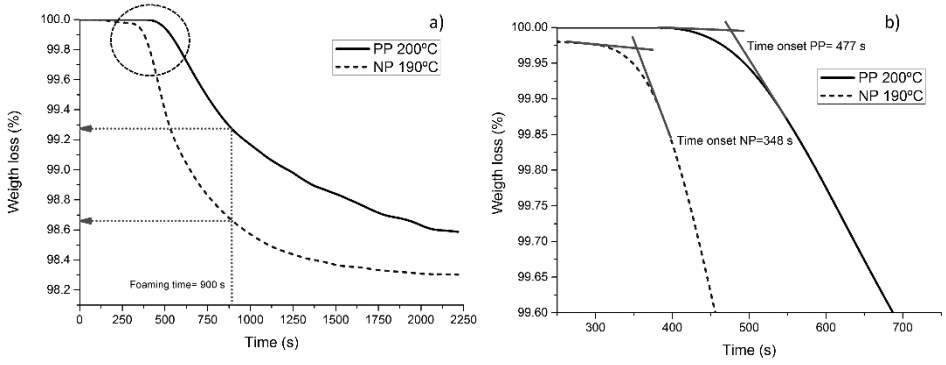

Figure 5: TGA isothermal scans. (a) Complete isotherms, (b) isotherms focused on the moment in which the ADC starts to decompose in gases.

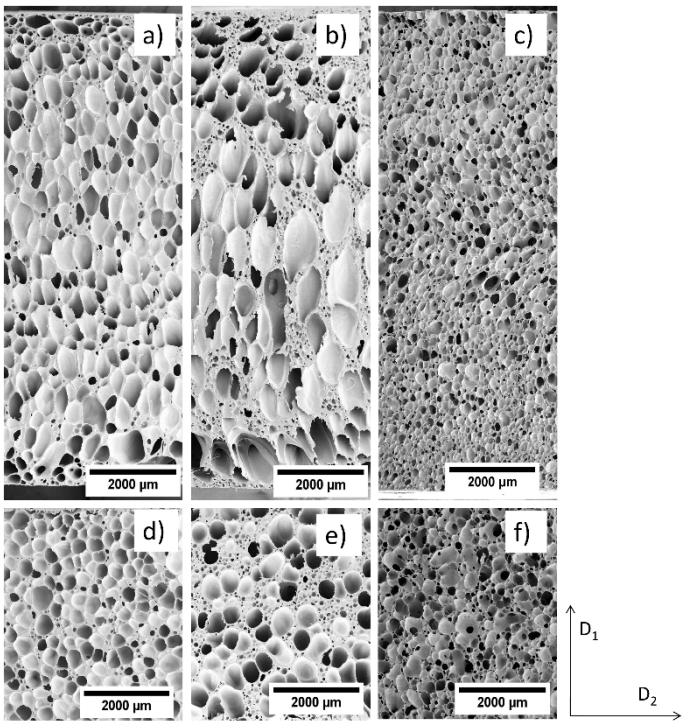

Figure 6: SEM images of some of the samples produced. Expansion plane (D1/D2): (a) PP0.5, (b) NP0.5, (c) NP8. Perpendicular to the expansion plane (D3/D2): (d) PP0.5, (e) NP0.5, (f) NP8.

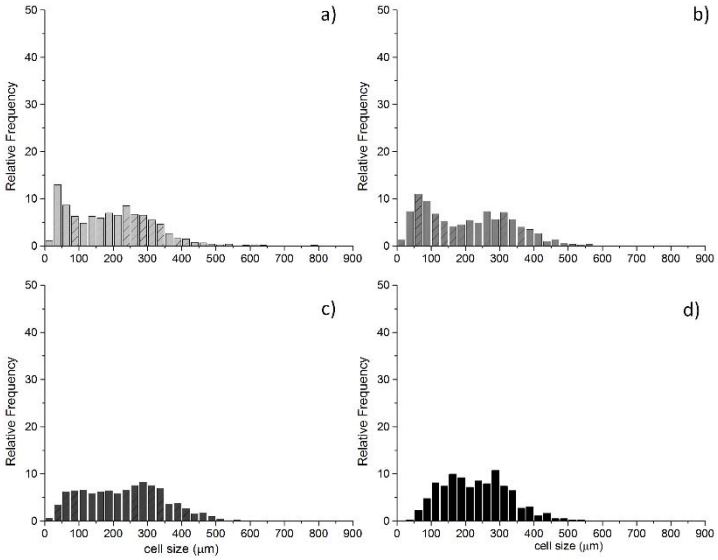

Figure 7: Cell size distributions of the unfilled PP foams. (a) PP0.5, (b) PP1.5, (c) PP4, and (d) PP8.

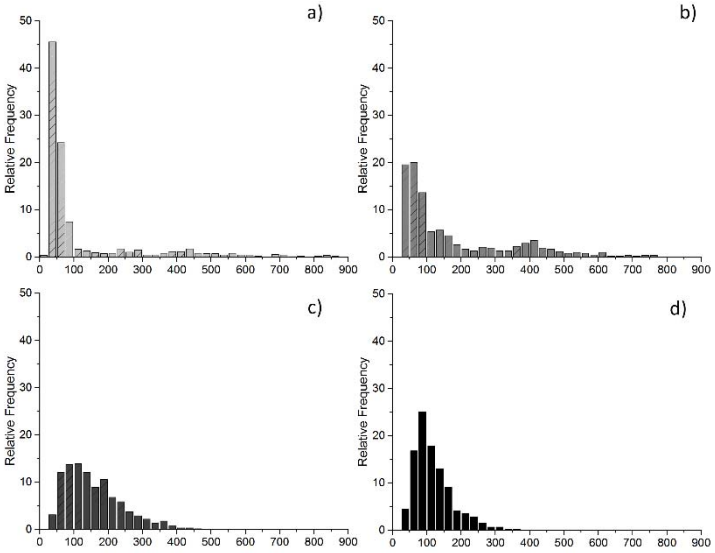

Figure 8: Cell size distributions of the nanoreinforced PP foams. (a) NP0.5, (b) NP1.5, (c) NP4, (d) NP8 (all of them in the same scale to facilitate their evaluation).

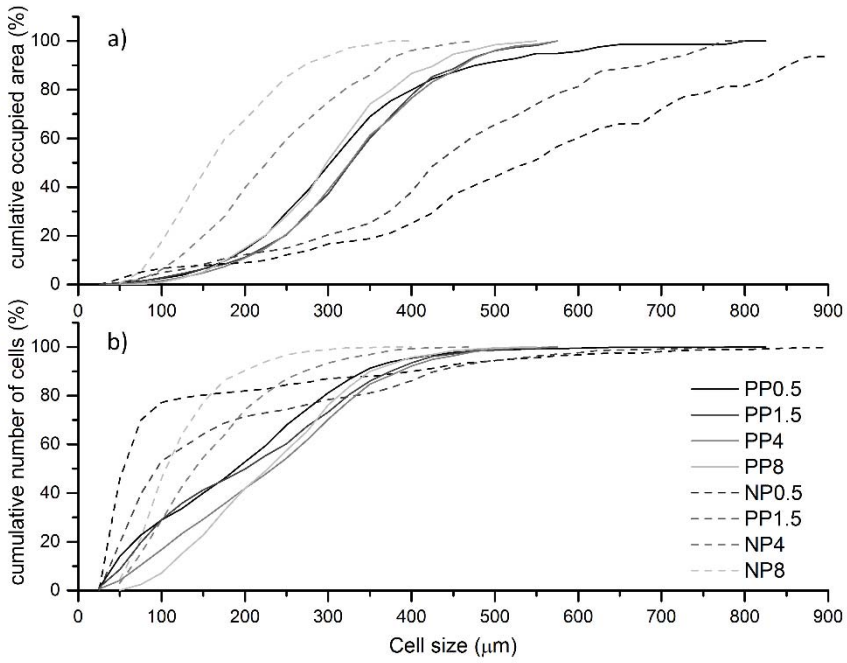

Figure 9: Cumulative curves of (a) occupied area and (b) number of cells.

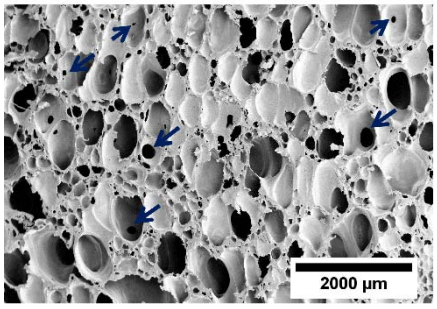

Figure 10: Cellular structure of the foam NP1.5. Arrows indicate broken cell walls.

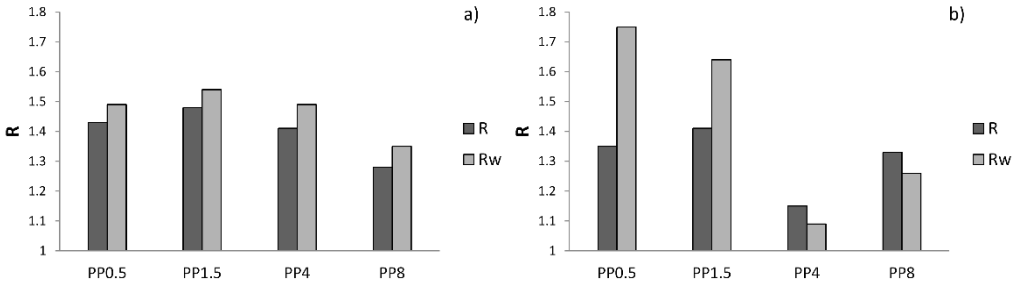

Figure 11: (a) R and Rw values of PP foams and (b) R and Rw values of NP foams.

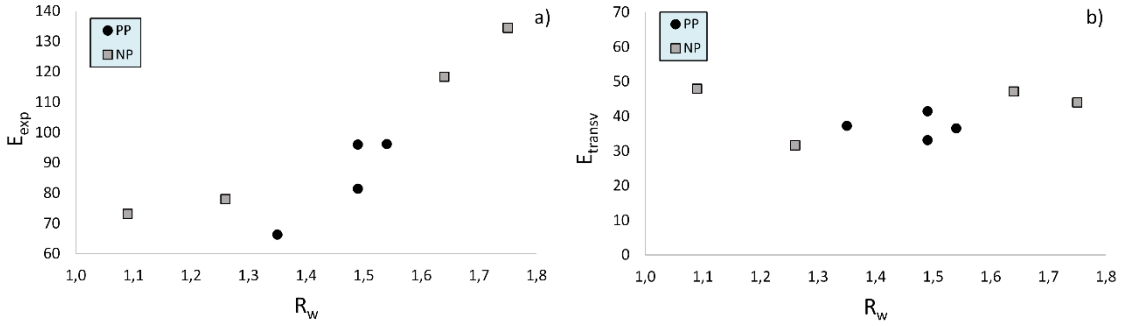

Figure 12: (a) E_{exp} versus R_w and (b) E_{transv} versus R_w.

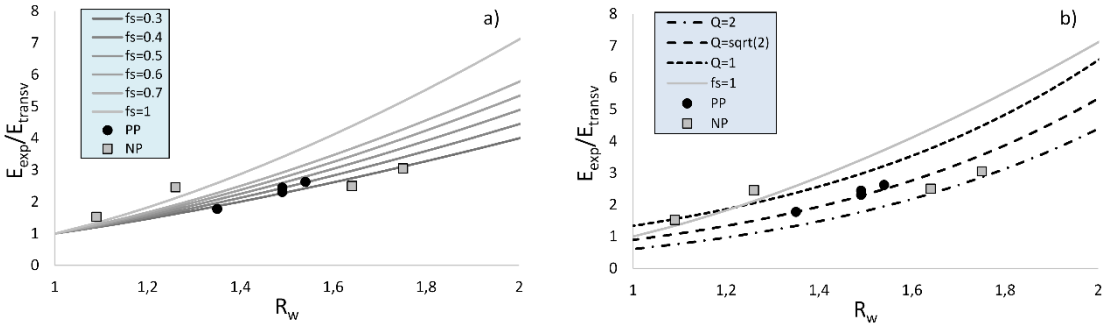
a)
fs=0.3
fs=0.4
fs=0.5
fs=0.6
fs=0.7
fs=1
PP
NP
E_{exp}/E_{transv}
R_w
b)
Q=2
Q=sqrt(2)
Q=1
fs=1
PP
NP
E_{exp}/E_{transv}
R_w

Figure 13:

[1] Klempner D, Frisch KC. Handbook of polymeric foams and foam technology. Hanser Publishers, 1991.
[2] Bouix R, Viot P, Lataillade JL. Polypropylene foam behavior under dynamic loadings; strain rate, density and microstructure effects. Int J Impact Eng. 2009;39:329-342.
[3] Zhai W, Kim YW, and Park CB. Steam-chest molding of expanded polypropylene foams. 1. dsc simulation of bead foam processing. Ind Eng Chem Res. 2010;49:9822-9829.
[4] Naguib HE, Park CB. Strategies for achieving ultra-low density polypropylene foams. Polym Eng Sci. 2002;42,1481-1492.
[5] Suh KW, Park CP, Maurer MJ, Tusim MH, Genova R, Broos R, Sophiea DP. Lightweight Cellular Plastics. Adv. Mater. 2000;12:1779-1789.
[6] Stange J, Münstedt H. Effect of long-chain branching on the foaming of polypropylene with azodicarbonamide. J Cell Plast. 2006;42:445-467.
[7] Naguib HE, Park CB. Strategies for achieving ultra low-density polypropylene foams. *Polym Eng Sci*. 2002;42:1481-1492.
[8] Nam GJ, Yoo JH, Lee JW. Effect of long-chain branches of polypropylene on rheological properties and foam-extrusion performances. J Appl Polym Sci. 2005;1793-1800.
[9] Lee LJ, Zeng C, Cao X, Han X, Shen J, Xu G. Polymer nanocomposite foams. Compos Sci Technol. 2005;65:2344-2363.
[10] Zhai W, Kuboki T, Wang L, Park CB. Cell structure evolution and the crystallization behavior of polypropylene/clay nanocomposites foams blown in continuous extrusion. Ind Eng Chem. 2010; 49:9834-9845.
[11] Zhai W. Park CB. Effect of nanoclay addition on the foaming behavior of linear polypropylene-based soft thermoplastic polyolefin foam blown in continuous extrusion. Polym Eng Sci. 2011;51: 2387-2399.
[12] Zheng WG, Lee YH, Park CB. Use of Nanoparticles for improving the foaming behaviors of Linear PP. J Appl Polym Sci. 2010;117, 2972-2979.
[13] Chaudhary AK, Jayaraman K. Extrusion of linear polypropylene–clay nanocomposite foams. Polym Eng Sci. 2011;51:1749-1756.
[14] Bhattacharya S, Gupta RK, Jollands M, Bhattacharya SN. Foaming behavior of high-melt strength polypropylene/clay nanocomposites. Polym Eng Sci. 2009;49:2070-2084.
[15] Nam PH, Maiti P, Okamoto M, Kotaka T. Foam processing and cellular structure of polypropylene/clay nanocomposites. Polym Eng Sci. 2002;42:1907-1918.
[16] Taki K, Yanagimoto T, Funami E, Okamoto M, Ohshima M. Visual observation of CO_2 foaming of polypropylene-clay nanocomposites. Polym Eng Sci. 2004;44:1004-1011.
[17] Oh K, Seo YP, Hong SM, Takahara A, Lee KH, Seo Y. Dispersion and reaggregation of nanoparticles in the polypropylene copolymer foamed by supercritical carbon dioxide. *Phys Chem Chem Phys*. 2013;15:11061-11069.
[18] Dolomanova V, Kumar V, Pyrz R, Madaleno LAO, Jensen LR, Rauhe JCM. Fabrication of microcellular pp-mmtnanocomposite foams in a sub-critical CO_2 process. Cell Polym.2012;31:125-144.
[19] Jiang XL, Bao JB, Liu T, Zhao L, Xu ZM, Yuan WK. Microcellular Foaming of Polypropylene/Clay Nanocomposites with Supercritical Carbon Dioxide. J Cell Plast.2009;45:515-538.
[20] Jiang M, Li HR, Fang D, Liu L, Tai QL, Li LC. Structure-Property Relationship in Injection Molded Polypropylene/Clay Composite Foams. Mater Manuf Processes. 2014;29:160-165.
[21] Antunes M, Velasco JI, Realinho V, Solorzano E. Study of the Cellular Structure Heterogeneity and Anisotropy of Polypropylene and Polypropylene Nanocomposite Foams. Polym Eng Sci. 2009;49: 2000-2413.
[22] Ma Y, Pyrz R, Rodriguez-Perez MA, Escudero J, Rauhe JC, Su X. X-ray microtomographic study of nanoclay-polypropylene foams. Cell Polym. 2011;30:90-110.

[23] Rodríguez-Pérez MA, Lobos J, Pérez-Muñoz CA, de Saja JA, González L, del Carpio BMA. Mechanical behaviour at low strains of LDPE foams with cell sizes in the microcellular range; advantages of using these materials in structural elements. Cell Polym. 2008;27:347-362.
[24] Rodríguez-Pérez MA, Lobos J, Pérez-Muñoz CA, de Saja JA. Mechanical Response of polyolefin foams with high densities and cell sizes in the microcellular range. J Cell Plast. 2009;45,389-403.
[25] Román-Lorza S. Formulación y caracterización de materiales celulares retardantes de llama libres de halógenos basados en poliolefinas. PhD Thesis. University of Valladolid,2010.
[26] Román-Lorza S, Rodríguez-Pérez MA, and de Saja JA. Cellular structure of halogen-free flame retardant foams based on LDPE. Cell Polym. 2009;28:249-268.
[27] Román-Lorza S, Rodríguez-Pérez MA, de Saja JA, Zurro J. Cellular structure of EVA/ATH halogen-free flame retardant foams. J Cell Plast. 2010;10:1-21
[28] Román-Lorza S, Sabadell J, García-Ruiz JJ, Rodríguez-Pérez MA, de Saja JA. Fabrication and characterization of Halogen Free Flame Retardant Polyolefin Foams. Mater Sci Forum. 2010; 636/637:98-205.
[29] Rodríguez-Pérez MA, Simões RD, Constantino CJL, de Saja, JA. Structure and physical properties of EVA/Starch precursor materials for foaming applications. J Appl Polym Sci.2011;212:2324-2330.
[30] Rodríguez-Pérez MA, Simões RDS, Román-Lorza M, Álvarez-Laínez C, Montoya-Mesa C, Constantino CJL, de Saja, JA. Foaming of eva/starch blends; characterization of the structure, physical properties and biodegradability. Polym Eng Sci. 2012;52:62-70.
[31] Gibson LJ, Ashby MF. Cellular Solids; Structure and Properties. 2th ed. Cambridge University Press; Cambridge, 1997.
[32] Christensen RM. Mechanics of low density materials. J Mech Phys Solids. 1986;34:563-578.
[33] Zhu HX, Knott JF, Mills NJ. Analysis of the elastic properties of open-cell foams with tetrakaidecahedral cells. J Mech Phys Solids.1997;45:319-343.
[34] Warren WE, Kraynik AM. Foam mechanics; The linear elastic response of two dimensional spatially periodic cellular materials. Mech Mater.1987;6:27-37.
[35] Huber AT, Gibson LJ. Anistropy of polymer foams. *J Mater Sci.* 1998;23: 3031-3040.
[36] Thomson, W. (Lord Kelvin).On the division of space with minimum partitional area.Philosphical magazine. 24, 503-514. 1887.
[37] Gong L, Kyriakides S, Jang WY. Compressive response of open cell foams. Part I; morphology and elastic properties. Int J Solids Struct.2005;42,1355-1379.
[38] Gong L, Kyriakides S, Triantafyllidis N. On the stability of kelvin cell foams under compressive loads. J Mech Phys Solids.2005;53:771-794.
[39] Sullivan RM, Ghosn LJ, Lerch, BAA. General tetrakaidecahedron model for open-celled foams. *Int J Solids Struct.*2008;45;1754-1765.
[40] Sullivan RM, Ghosn LJ. Shear moduli for non-isotropic, open cell foams using a general elongated Kelvin foam model. *Int J Eng Sci*. 2009;47:990-1001.
[41] Hamilton AR, Thomsen OT, Madaleno LAO, Jensen LR, Rauhe JCM, Pyrz R. Evaluation of the anisotropic mechanical properties of reinforced polyurethane foams. *Comp Sci Tech*. 2013;87: 210-217.
[42] Pinto J, Solórzano E, Rodriguez-Perez MA, de Saja JA. Characterization of the cellular structure based on user-interactive image analyses procedures. *J Cellr Plast*. 2013;49:555-575.
[43] Kumar V. Process synthesis for manufacturing microcellular thermoplastic parts. PhD. Thesis. Massachusetts Institute of Technology: Cambridge MA, 1988.
[44] Weller JE, Kumar V. Solid-state microcellular polycarbonate foams. I. The steady-state process space using subcritical carbon dioxide. Polym Eng Sci. 2010;50:2160-2169.
[45] Bhatti AS, Dollimore D. The thermal decomposition of azodicarbonamide. *Thermochim Act*a. 1984;76:63-67.
[46] Spitael P, Macosko CW. Strain hardening in polypropylenes and its role in extrusion foaming. Polym Eng Sci. 2004;2090-2100.

[47] Laguna-Gutierrez E, Lopez-Gil A, Saiz-Arroyo C, Van Hooghten R, Moldenaers P. Rodriguez-Perez, MA. Extensional rheology/cellular structure/mechanical behaviour relationships in HMS PP/montmorillonite foams. Unpublished results.

[48] Lee ST, Park CB, Ramesh NS. Polymeric Foams. Science and Technology: Taylor and Francis Group, 2007.

[49] Bao JB, Liu T, Zhao L, Hub GHA. Two-step depressurization batch process for the formation of bi-modal cell structure polystyrene foams using $scCO_2$. J Supercrit Fluids. 2011;55:1104-1114.

[50] Fazekas A, Dendievel R, Salvo L, Bréchet Y. Effect of microstructural topology upon the stiffness and strength of 2D cellular structures. Int J Mech Sci. 2002;44:2047-2066.